SCIENTIFIC JOURNAL OF MARITIME RESEARCH [POMORSTVO]
University of Rijeka FACULTY OF MARITIME STUDIES

https://doi.org/10.31217/p.40.2.8

Optimization of Cleaning Blades for Underwater Biofouling Removal Robots

Xiaochang Shi[1], Changsheng Yang[2], Wenbin Ma[3*]

[1] Faculty of Mechatronic Engineering, Hainan University, Hainan, P.R. China, e-mail: xiaochang.shi@hainanu.edu.cn
[2] Faculty of Information and Communication Engineering, Hainan University, Hainan, P.R. China, e-mail: 23210810000030@hainanu.edu.cn
[3] Faculty of Marine Science and Engineering, Hainan University, Hainan, P.R. China, e-mail: wenbinma_edu@163.com
[*] Corresponding author

ARTICLE INFO

Original scientific paper
Received 5 November 2025
Accepted 1 February 2026

Key words:
Biofouling
Barnacle removal
Design Optimization
Underwater robot
Cutting theory

ABSTRACT

To address the issues of increased resistance and energy consumption caused by biofouling on ship hulls, a scraping blade design method based on cutting theory is proposed for a model of an underwater robot. A dynamic model of the blade is established by combining classical cutting theory and extrusion cutting theory, and the analysis indicates that a rake angle of 20° satisfies the removal requirements of barnacles while reducing resistance and energy consumption. On this basis, an idealized attachment model of barnacles and ship hulls is constructed in ABAQUS to perform finite element simulations for single barnacle, double barnacles, and various distribution patterns, including aligned, staggered, and dense multi-barnacle arrangements. The results demonstrate that the blade generates stresses significantly higher than the maximum adhesion strength of barnacles under all conditions, confirming the feasibility of the 20° rake angle. Compared with ultrasonic cavitation cleaning, the proposed method achieves higher cleaning efficiency, lower energy demand, and better environmental compatibility, providing an effective and sustainable solution for ship hull maintenance.

1 Introduction

Barnacles are small marine crustaceans [1] that typically attach themselves to hard surfaces such as rocks, pier piles, ship hulls, buoys, and even the bodies of whales and sea turtles. Their attachment can cause various negative impacts on ships and marine engineering structures. A large number of barnacles significantly increase underwater resistance, resulting in higher fuel consumption and potential damage to surface materials of marine structures. For example, on a 100,000-ton oil tanker under moderate biofouling conditions, hydrodynamic drag can increase by up to 30%, leading to an additional fuel consumption of approximately 12 tons per day, which directly elevates operating costs and sharply increases carbon emissions [2]. In addition, barnacle adhesion disrupts the hydrodynamic characteristics of ship hulls and alters surface metal properties, thereby accelerating corrosion [3]. For underwater observation instruments, especially high-precision sensors, microbial fouling can degrade measurement accuracy, while barnacle settlement can drastically shorten the service life of such equipment [4].

Cleaning barnacles from ship hulls is typically performed in dry docks [5], mainly using high-pressure water jets, scrapers, or chemical agents to remove fouling and rust from the hull surface. However, dry-dock cleaning is costly and time-consuming, may damage antifouling coatings, negatively affects fuel efficiency, and generates pollutants that can impact the environment. Since the 1960s, in order to improve barnacle removal efficiency, researchers worldwide have developed underwater cleaning devices operated by divers. Nevertheless, due to complex and unpredictable underwater conditions, divers face considerable risks and challenges during such operations. To further reduce human la-

Table 1 Attachment of barnacles at different stages.

Stage	Attachment Type	Removal Force / N	Strength / MPa
Glandular juvenile	Temporary adhesion	< 0.001	0.16–0.29
Glandular larvae	Permanent adhesion	< 0.019	0.94
Shell juvenile	Permanent adhesion	< 0.350	0.18
Adult barnacle	Permanent adhesion	< 180	0.94

bor and enable autonomous removal of biofouling from ship hulls, intelligent underwater cleaning technologies have subsequently emerged [5].

Jotun, in collaboration with Kongsberg Maritime, has developed the Hull-Skater cleaning robot, which uses a rotating brush system for hull cleaning and is equipped with four magnetic wheels for flexible maneuvering. However, its adhesion and cleaning performance remain limited on surfaces with high curvature or complex geometries [6]. The Naval Academy of Tunisia proposed the ARMROV underwater cleaning solution, which utilizes a robotic manipulator to cover hull areas underwater, reducing operational difficulty and energy consumption, though it is restricted to vessels of specific tonnage [7]. South Korea's SLM Corporation introduced the CHIRO cleaning system, capable of completing hull-cleaning operations on a 300-meter commercial vessel within eight hours [8]. Remora Technology, a company based in Turkey, released the Neta underwater cleaning robot, which employs a combination of crawler tracks and propeller propulsion and can be controlled via a mobile application [9].

Research in this field started relatively late in China. The Kunming Haiwei Electromechanical Research Institute developed the SQ-101 underwater cleaning device, which uses thrusters for hull adhesion and caterpillar-style locomotion, although its cleaning efficiency remains low [10]. Qingdao Feimabin Company introduced a flexible negative-pressure cavitation system, using seawater as the working medium [11]. Harbin Banzhilan Company released the BLUCR series, with the No. 3 and No. 4 prototypes completing cleaning trials at Tangshan Port in March 2022 [12]. Tianjin Hanhai BlueSail launched the JH-IV hull-cleaning robot, which can be equipped with a variety of cleaning brush discs to remove barnacles under different operational scenarios, achieving a cleaning rate as high as 900 m^2/h [13]. However, all the above hull-cleaning robots rely on rotating brush technology or negative-pressure cavitation, and their effectiveness in removing barnacles remains insufficient. Wang et al. employed orthogonal cutting theory and the Peel-Zone method to design a marine steel-pile cleaning robot and developed a cutting-force model, validated by finite element simulations with an error of less than 15%. Their analysis showed that the rake angle has a significant influence on cleaning performance, and they recommend avoiding excessive reduction of the rake angle during tool design [14]. At present, the use of blade-based barnacle removal in hull-cleaning robots has been mentioned only in patents or theoretical studies, with no in-depth research available.

Based on the investigation of barnacle adhesion at different physiological stages, the relevant parameters are summarized in Table 1 [15]. According to the data, once barnacles reach adulthood, the maximum force required for removal can reach 180 N, corresponding to an adhesion strength of 0.94 MPa. Therefore, if the designed cleaning mechanism is capable of applying a removal stress exceeding 0.94 MPa, it can effectively achieve hull surface cleaning [16]. In this study, adult barnacles are taken as the primary research object. A barnacle model and a cleaning-blade mechanism for a barnacle-removal robot are established to analyze the influence of the tool rake angle on cutting force and to determine the optimal rake angle. Subsequently, the cleaning stress corresponding to the optimal rake angle is simulated in ABAQUS and compared with the barnacle adhesion strength (0.94 MPa) to verify the theoretical cleaning capability of the mechanism. The findings aim to provide a reference for optimizing the tool design of barnacle-cleaning robots.

2 Design Principle of the Barnacle-Cleaning Robot

This study proposes a barnacle-cleaning robot for ship hull maintenance, and its overall structure is shown in Figure 1. The robot is equipped with magnetic crawler tracks and thrusters, enabling stable adhesion to the hull surface and flexible mobility to accommodate complex curved geometries. In low-visibility underwater environments, an integrated lighting system provides sufficient illumination, effectively improving operational visibility. A high-definition camera mounted on the robot captures real-time images of the hull surface, which are transmitted to the land-based control terminal via an image transmission module. Combined with a target recognition algorithm, the system can accurately identify and locate barnacle attachments on the hull surface.

A cleaning blade is installed at the front end of the robot to mechanically remove barnacles using the extrusion-cutting method. By integrating orthogonal cutting theory with an extrusion failure mechanism, this

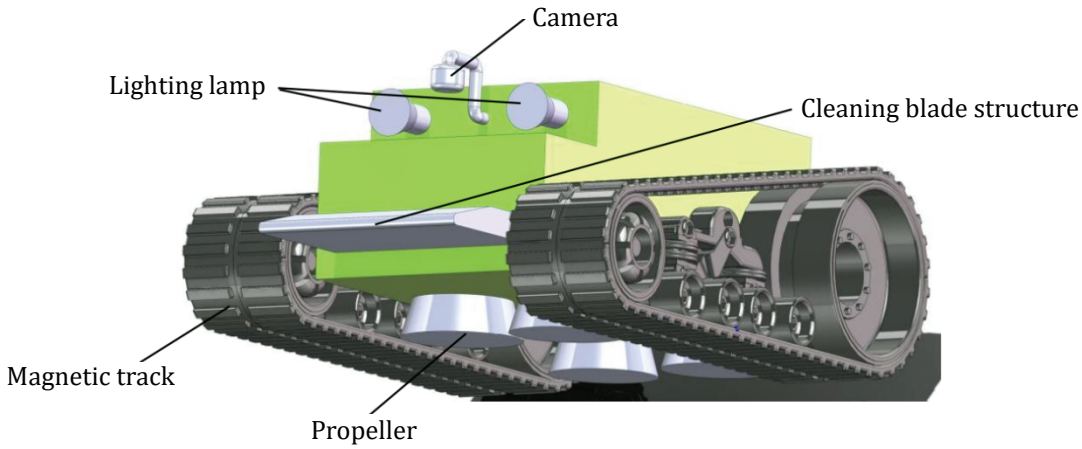

Figure 1 Barnacle-cleaning robot model.

cleaning approach ensures high removal efficiency while minimizing potential damage to the hull structure. As a result, the system achieves efficient and safe barnacle removal operations.

When barnacle removal is required, the robot is deployed onto the hull surface, typically starting from the waterline or areas with severe fouling. An electromagnetic crawler adhesion system is installed on the underside of the device. Once the robot contacts the steel hull, the electromagnets are energized to generate a strong magnetic field, ensuring stable adhesion. This enables fully independent underwater operation without any external support structures. Steering and trajectory planning are achieved through differential speed control of the left and right crawler tracks, allowing autonomous navigation along the hull surface and effective adaptation to complex geometries, including curved, uneven, and inclined regions.

Four thrusters are mounted at the bottom corners of the robot, with thrust vectors oriented perpendicular to the hull surface. These thrusters are primarily used to support attachment and detachment maneuvers. Once stable adhesion is established and the cleaning task begins, the thrusters remain inactive in terms of propulsion. During movement, an onboard high-definition camera is activated to capture real-time images of the hull surface. The acquired images are processed by an integrated image-recognition module, where a target-detection algorithm identifies and locates barnacle attachment regions. The resulting positional information is then transmitted to guide the cleaning unit for precise operation.

Upon completion of target recognition, the cleaning blade mounted at the front of the robot is engaged. The blade operates based on the extrusion-cutting mechanism, whereby contact is established with the barnacle at a prescribed angle, allowing the shell structure to be sheared and peeled away to achieve efficient removal. The cutting strategy is designed with full consideration of force orientation and hull material tolerance, ensuring effective barnacle elimination while preventing surface scratches or structural damage. To address limited visibility in the underwater environment, an auxiliary illumination module is automatically activated to enhance lighting conditions, improving both recognition accuracy and cleaning precision.

Throughout the cleaning process, real-time imagery and operation data are transmitted to the land-based control terminal, enabling continuous monitoring and adaptive strategy adjustment by the operator. After completing a designated cleaning region, the robot autonomously moves to the next area and repeats the procedure until the entire hull surface has been processed. Once all tasks are completed, the robot returns to the initial deployment position and is subsequently retrieved at the water surface by the operator.

3 Method and Model

3.1 Cleaning Blade Dynamics Model

Barnacles adhere firmly to rigid substrates through secreted adhesive substances, and a hardened calcareous shell gradually forms above the adhesive layer. The longer the adhesion time, the stronger the bonding becomes, which significantly increases the difficulty of removal. Although conventional cutting tools offer high sharpness, they tend to damage the hull during barnacle removal and exhibit relatively short service life. Therefore, in this study, a classical cutting approach is adopted in combination with extrusion-cutting methods [17], and a theoretical analysis is carried out by utilizing the extrusion effect generated by a blunt, rounded cutting edge.

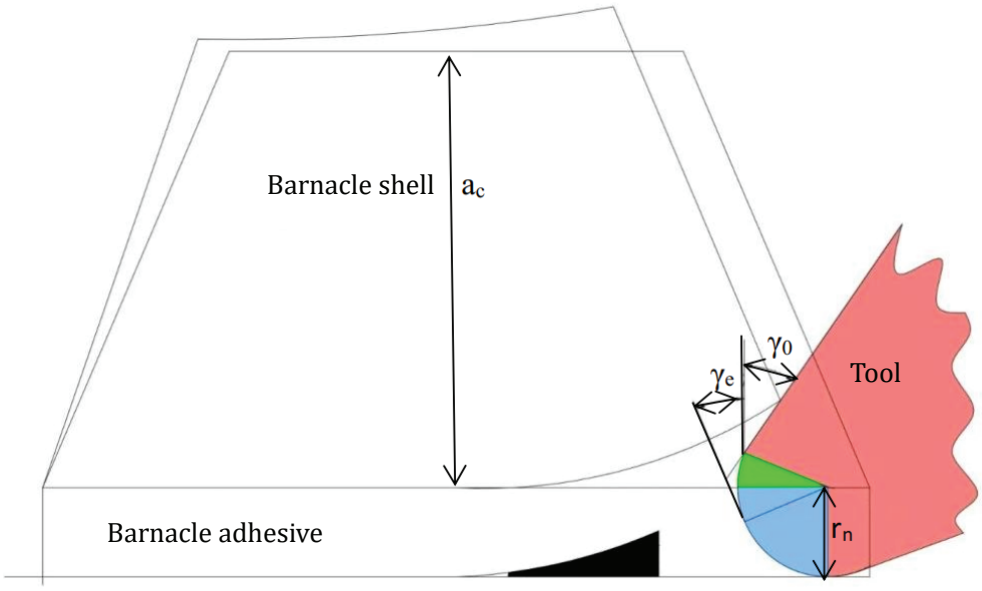

Figure 2 Cutting Force Model, γ_0 is the theoretical rake angle, γ_e is the effective rake angle, a_c is the height of the barnacle, r_n is the radius of the flat edge.

During the extrusion-cutting process, the theoretical rake angle may not participate in the actual cutting action, because the cutting thickness is on the same order of magnitude as the radius of the Tool Blunt Round Edge (TBRE). In this case, the cutting force is generated by the effective rake angle of the TBRE. As illustrated in Figure 2, the angle between the tangential direction at the barnacle–TBRE contact point and the normal direction is defined as the effective rake angle at the contact point.

$$\gamma_e = \begin{cases} \arcsin\left(\frac{|r_n - a_c|}{r_n}\right), a_c \le r_n(1+\sin\gamma_0) \\ \gamma_0, a_c > r_n(1+\sin\gamma_0) \end{cases} \quad (1.1)$$

where γ_e is the effective rake angle, r_n is the edge radius, h is the barnacle height, and γ_0 is the theoretical rake angle.

The total cutting force acting on the tool is mainly composed of three components: the extrusion force generated by compressive action, the shear force produced during material shearing, and the frictional force induced by sliding at the tool–barnacle interface.

$$F = F_p + F_s + F_f \quad (1.2)$$

where F is the total cutting force, F_p is the extrusion force, F_s is the shear force, and F_f is the friction force.

The extrusion force is generated during the extrusion-cutting process by the combined compressive action of the Tool Blunt Round Edge (TBRE) and the effective rake-angle region, which induces localized compressive stress on the barnacle material. To estimate the extrusion force, this study employs an approximate method based on the contact area and the corresponding stress distribution.

$$F_p = 9.8k\sigma_{eq}a_w r_n \theta_p \frac{\pi}{180} \quad (1.3)$$

where k=0.204 is a correction coefficient [17], σ_{eq}=0.94 is the equivalent compressive strength of the barnacle material, a_w is the cutting width, and ω denotes the extrusion angle range.

Due to the presence of a tool rake angle introduced by practical manufacturing and processing constraints, the extrusion force range must be divided into two regions according to the relationship between the cutting depth and the TBRE.

$$\theta_p = \begin{cases} \arccos\left(\frac{(r_n - a_c)}{r_n}\right), a_c \le r_n \\ \frac{\pi}{2} + \gamma_e, r_n \le a_c \end{cases} \quad (1.4)$$

During the shearing process, the instantaneous effective rake angle varies at each position along the cutting path and therefore cannot be represented by a single unified value. Instead, it must be determined according to the local material position at that moment. Thus, the instantaneous effective rake angle at any given point is expressed as

$$\gamma_e = \arcsin(\cos\theta) \quad (1.5)$$

When calculating the shear force, the shear force at each position should be evaluated individually and subsequently superimposed to obtain the total shear force.

$$F_{sx}=\begin{cases}\int_0^{\arccos\left(1-\frac{a_c}{r_n}\right)}\frac{r_n\tau_s a_w\cos(\beta-\gamma_e)}{\sin\varphi\cos(\varphi+\beta-\gamma_e)}\sin\theta\,d\theta, a_c\le r_n\\ \int_{\frac{\pi}{2}}^{\frac{\pi}{2}+\gamma_e}\frac{r_n\tau_s a_w\cos(\beta-\gamma_e)}{\sin\varphi\cos(\varphi+\beta-\gamma_e)}\sin\theta\,d\theta, r_n\le a_c\le r_n(1+\sin\gamma_0)\\ [a_c-r_n(\sin\gamma_0+1)]\frac{\tau_s a_w\cos(\beta-\gamma_e)}{\sin\varphi\cos(\varphi+\beta-\gamma_e)}, r_n(1+\sin\gamma_0)\le a_c\end{cases} \quad (1.6)$$

Using the same approach, the shear force in the y-axis can be expressed as

$$F_{sy}=\begin{cases}\int_0^{\arccos\left(1-\frac{a_c}{r_n}\right)}\frac{r_n\tau_s a_w\sin(\beta-\gamma_e)}{\sin\varphi\cos(\varphi+\beta-\gamma_e)}\sin\theta\,d\theta, a_c\le r_n\\ \int_{\frac{\pi}{2}}^{\frac{\pi}{2}+\gamma_e}\frac{r_n\tau_s a_w\sin(\beta-\gamma_e)}{\sin\varphi\cos(\varphi+\beta-\gamma_e)}\sin\theta\,d\theta, r_n\le a_c\le r_n(1+\sin\gamma_0)\\ [a_c-r_n(\sin\gamma_0+1)]\frac{\tau_s a_w\sin(\beta-\gamma_e)}{\sin\varphi\cos(\varphi+\beta-\gamma_e)}, r_n(1+\sin\gamma_0)\le a_c\end{cases} \quad (1.7)$$

3.2 Establishment of the Idealized Barnacle Model

Based on a review of relevant literature and on-site investigations, it was found that an adult barnacle is primarily composed of two parts: a calcareous shell and an adhesive base. In general, the diameter of a mature barnacle is approximately 10 mm, while larger individuals may reach up to 50 mm. To improve the reliability of the geometric modeling, barnacle samples with relatively uniform morphology and dense distribution were selected from nearshore regions. A micrometer was used for dimensional measurements, and a systematic sampling method was employed to record key geometric parameters, including maximum diameter, minimum diameter, and vertical height.

The collected measurements were statistically processed to obtain the mean values of each dimension, as summarized in Table 2. On this basis, to enhance mesh quality and reduce computational complexity during finite element simulation, multiple iterations of geometric adjustment and verification were conducted. The finalized parameters of the idealized barnacle model used in subsequent simulations are presented in Table 3.

Table 2 Sampling average size of barnacles.

$\overline{D_1}$ (mm)	$\overline{D_2}$ (mm)	$\overline{R_1}$ (mm)	$\overline{R_2}$ (mm)	$\overline{H}$ (mm)	$\overline{B}$ (mm)
10.46	6.53	5.23	3.27	8.48	1.47

Table 3 Dimensions of the Idealized Barnacle Model.

D_1 (mm)	D_2 (mm)	R_1 (mm)	R_2 (mm)	H (mm)	B (mm)
10.5	6.5	5.25	3.25	8.5	1.5

Where D_1 is the diameter of the larger circular cross-section of the idealized barnacle model, D_2 is the diameter of the smaller circular cross-section, R_1 and R_2 are the corresponding radii, H is the height of the idealized barnacle model, and B is the shell wall thickness. Based on the pressure formula and the removal force of adult barnacles listed in Table 1, the barnacle–substrate contact area is calculated to be 191.4 mm^2. Using the circular area equation, the corresponding contact radius between the barnacle cement and the hull surface is approximately 7.8 mm [16].

4 Results and Discussion

4.1 Results and Analysis of the Cleaning Blade Dynamics Model

By solving the proposed model, the relationship between the rake angle and cutting force was obtained, as illustrated in Fig. 3. As shown in the figure, the rake angle has a significant influence on the cutting force. When the rake angle is within the range of (0°, 50°), a smaller rake angle results in a larger required cutting force. In the range of [50°, 90°), the cutting force varies more gradually with respect to the rake angle. When the rake angle is approximately 20°, the corresponding cutting force is close to the maximum force required for barnacle removal (180 N). During the cleaning process, the cutting force generated by the cleaning blade will cause equal but opposite reaction forces. As the cutting force increases, the reaction force will also increase, which will not only accelerate the wear of the blade, but also increase the resistance and energy consumption of the barnacle cleaning robot during the propulsion process [18]. On the contrary, if the tool rake angle design is unreasonable and results in too little cutting force, it will be difficult to effectively break the hard shell structure of adult barnacles , thereby reducing cleaning efficiency. Taking into account the removal requirements of barnacles and the service life of cutting tools, 20° was ultimately selected as the optimized rake angle parameter for cleaning tools.

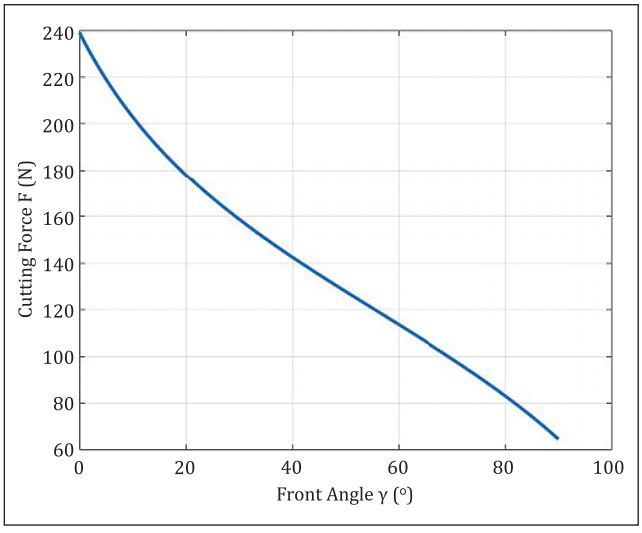

Figure 3 Relationship between Front Angle and Cutting Force.

4.2 Finite Element Analysis of Barnacle Cleaning

A finite element simulation was conducted on a single barnacle adhering to the ship hull surface to evaluate the cleaning forces, and the entire model was constructed and analyzed using ABAQUS. In the model, a rectangular steel plate was employed beneath the barnacle to represent the ship hull surface, with dimensions of 200 mm in length, 200 mm in width, and 20 mm in thickness. After completing the geometry, material parameters were assigned based on field observations and literature. The barnacle shell was defined with a density of 5000 kg/m^3, a Young's modulus of 1×10^{11} Pa, and a Poisson's ratio of 0.3, while the barnacle cement layer was defined with a density of 1190 kg/m^3, a Young's modulus of 3×10^9 Pa, and a Poisson's ratio of 0.1. Both the ship hull and cleaning blade were modeled as steel, with a density of 7850 kg/m^3 and a Young's modulus of 2×10^{11} Pa [16]. The hull plate was subjected to a fixed boundary condition, and the rake angle of the cleaning blade was set to 20°. The simulation assumed a static fluid environment surrounding the barnacle. To ensure the reliability of the numerical results, a custom meshing strategy was applied. Tetrahedral elements with a refined mesh size were used for both the barnacle shell and cement layers to accurately capture local deformation responses.

During the cleaning process, the ideal condition is that the blade directly engages with the exposed lower region of the barnacle shell. However, in practical scenarios, sufficient contact with the shell base is often difficult to achieve. Therefore, a single generatrix on the barnacle surface was selected, and six discrete contact locations were defined along this line from the base upward for simulation analysis. The results are illustrated in Fig. 4.

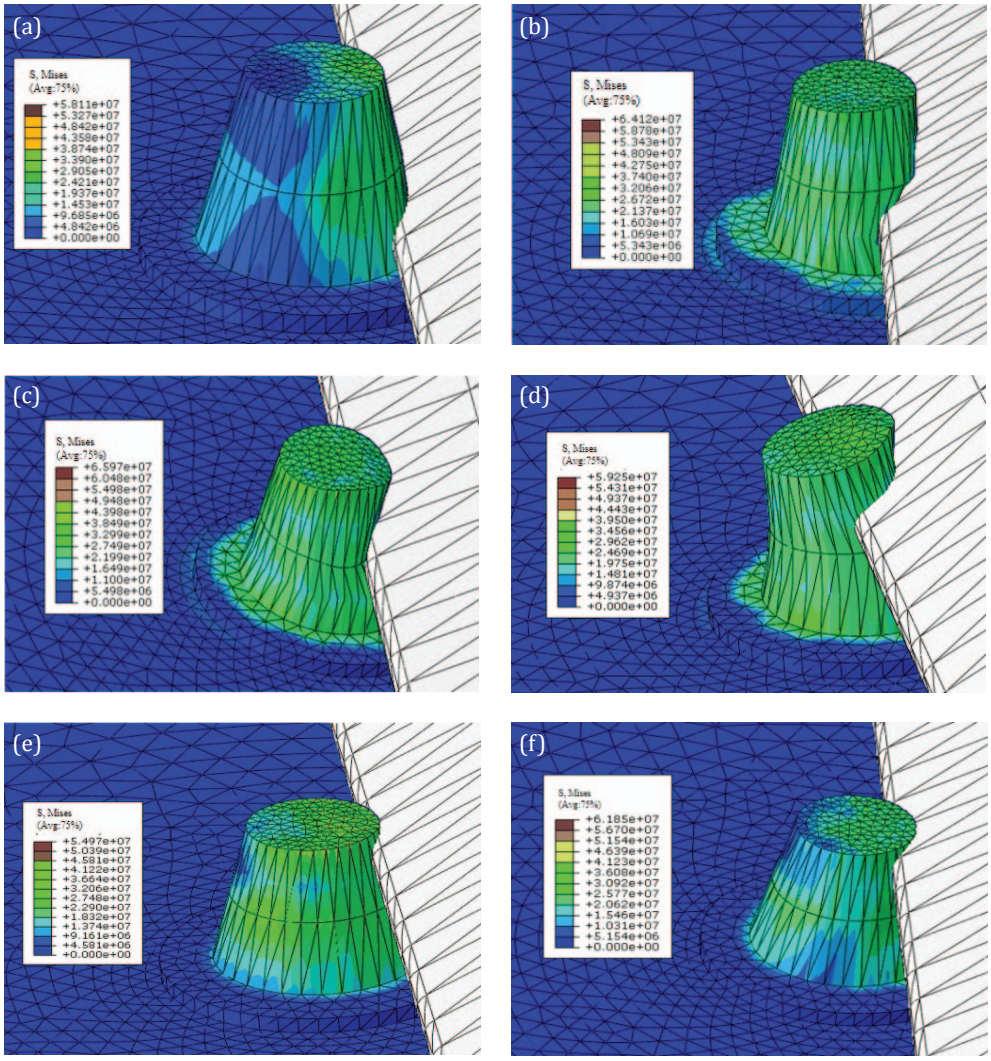

Figure 4 Cleaning Stress on the Barnacle Adhesive Base-Hull Contact Interface: (a) Blade directly contacting barnacle shell base; (b) Contact point 1.5 mm from shell base; (c) Contact point 3.0 mm from shell base; (d) Contact point 4.5 mm from shell base; (e) Contact point 6.0 mm from shell base; (f) Contact point 7.5 mm from shell base.

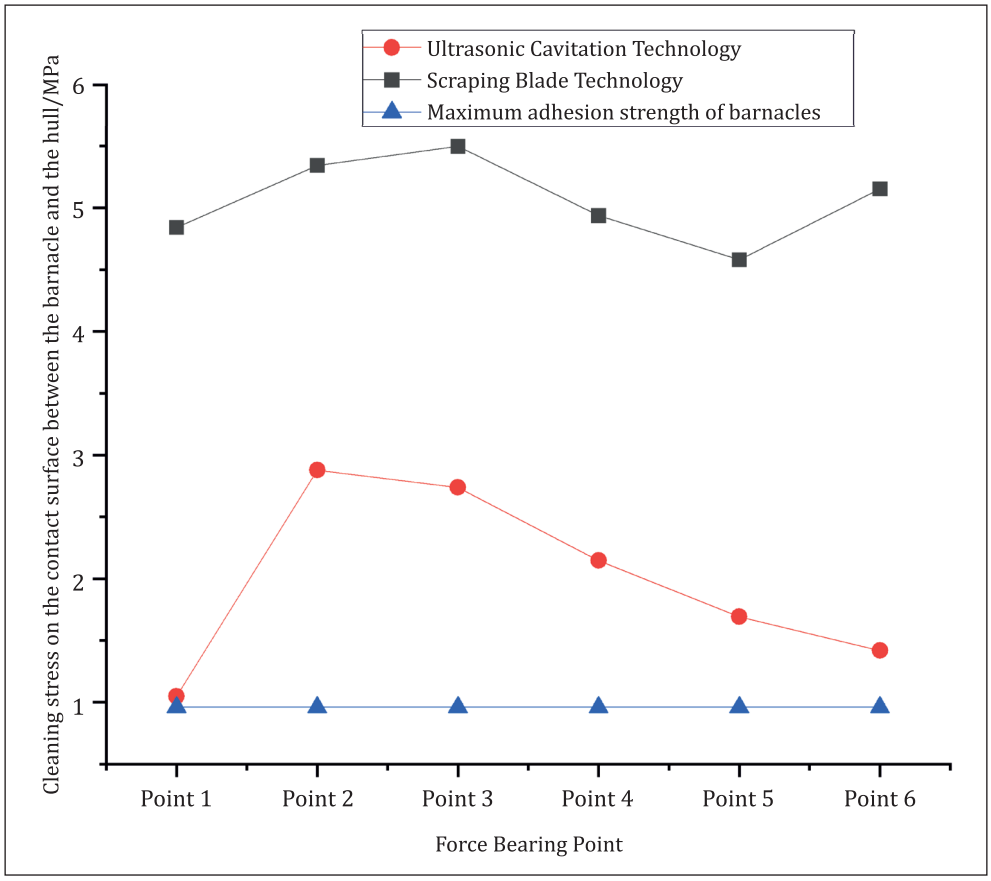

Figure 5 Minimum cleaning stress lines generated by different cleaning techniques.

For further evaluation, the obtained stress results were compared with those of ultrasonic cavitation cleaning technology currently used in hull-cleaning robots [16]. The stress evolution for both methods was then plotted for comparison, as shown in Fig. 5.

From the simulation results in Fig. 4, it can be observed that the minimum cleaning stress for a single barnacle reaches 4.581 MPa, which is more than four times the maximum adhesion strength between the barnacle and the hull. Meanwhile, the barnacle model exhibits a noticeable deformation response. This indicates that, under the current blade parameter settings, the stress induced by the cleaning blade sufficiently exceeds the adhesion threshold at the barnacle–substrate interface, thereby enabling effective interfacial failure and ensuring reliable barnacle removal.

As shown in Fig. 5, the blue curve represents the maximum adhesion strength between the barnacle and the hull, the red curve represents the cleaning stress generated by ultrasonic cavitation technology during barnacle removal [16], and the gray curve corresponds to the stress profile produced by the cleaning blade model. The results demonstrate that the cleaning stress generated by the blade is approximately twice that of ultrasonic cavitation, and its minimum stress value still remains significantly higher than the barnacle's maximum adhesion strength. Considering that barnacles on ship hulls predominantly exist in their adult form, and that the cleaning efficiency of ultrasonic cavitation for mature barnacles is only about 30%, the proposed blade-based cleaning method exhibits clear advantages in both stress output and removal efficiency. It should be noted that the comparison between the two cleaning techniques in this article is mainly based on mechanical response characteristics and cleaning stress levels, with a focus on verifying the feasibility and effectiveness of the cleaning knife technology in overcoming barnacle adhesion, without involving engineering quantitative indicators such as unit area cleaning energy consumption and cleaning time. In addition to effectively overcoming barnacle adhesion and achieving thorough removal, the stress generated by the blade is concentrated at the barnacle–substrate interface, minimizing its influence on the hull surface. This indicates superior safety and engineering feasibility compared with ultrasonic cavitation removal.

Based on the above results, a dual-barnacle adhesion model was further developed to evaluate the adaptability and cleaning stability of the blade in more complex fouling scenarios. This extended model forms the foundation for subsequent simulations involving different

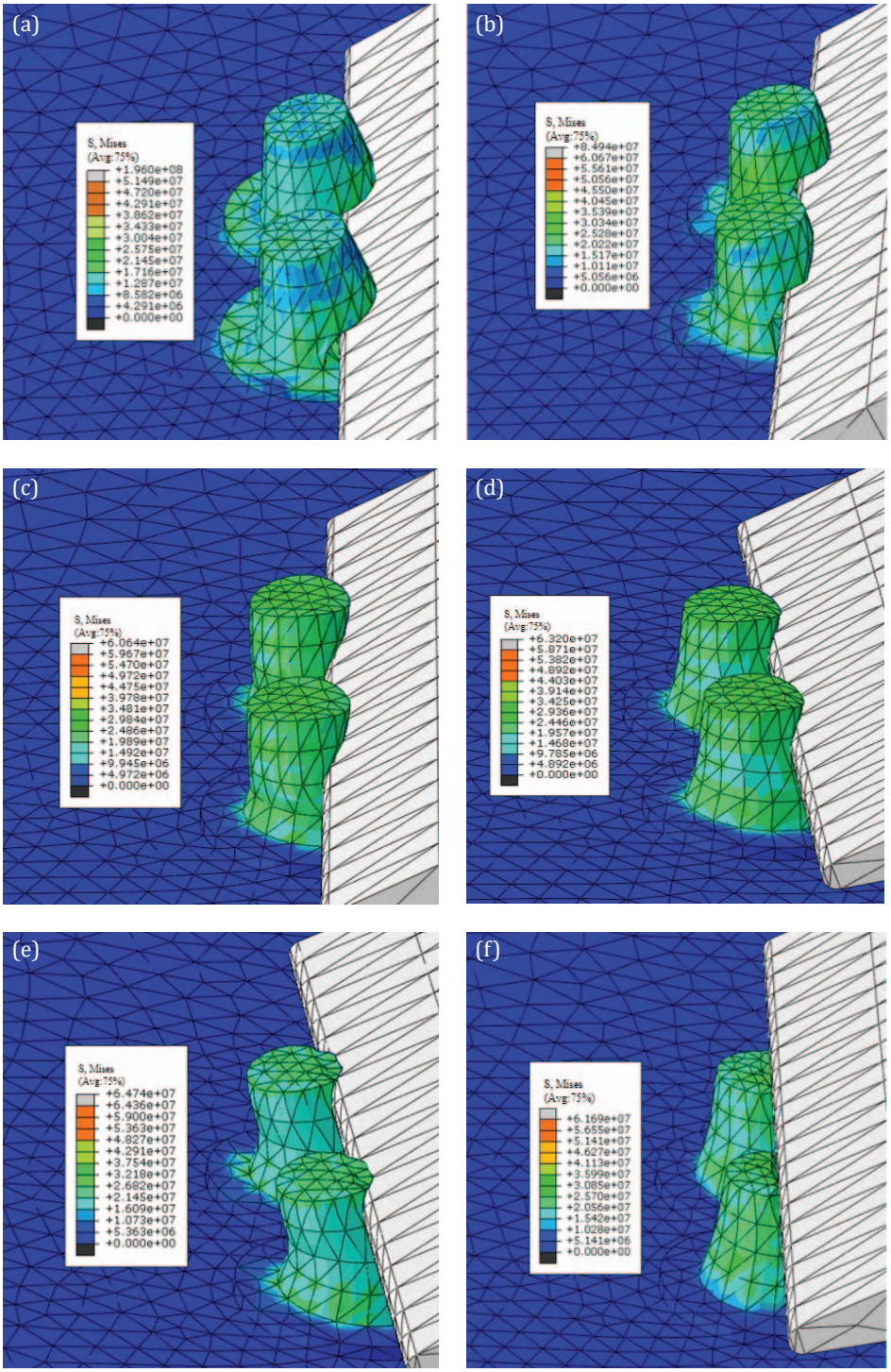

Figure 6 Cleaning Stress on Dual Barnacles' Adhesive Base-Hull Contact Interface: (a) Blade directly contacting barnacle shell bases; (b) Contact point 1.5 mm from shell bases; (c) Contact point 3.0 mm from shell bases; (d) Contact point 4.5 mm from shell bases; (e) Contact point 6.0 mm from shell bases; (f) Contact point 7.5 mm from shell bases.

barnacle distributions and quantities (e.g., collinear arrangements, random staggered distributions, or densely clustered formations). Aside from the addition of a second barnacle, all other simulation parameters remained consistent with those used in the single-barnacle model. The stress distribution generated at the cement–substrate interface is shown in Fig. 6, and the corresponding stress-variation curve is plotted in Fig. 7.

As shown in Fig. 7, the cleaning stresses generated by the blade model for both the single- and double-barnacle cases remain consistently at approximately four times the maximum adhesion strength between the bar-

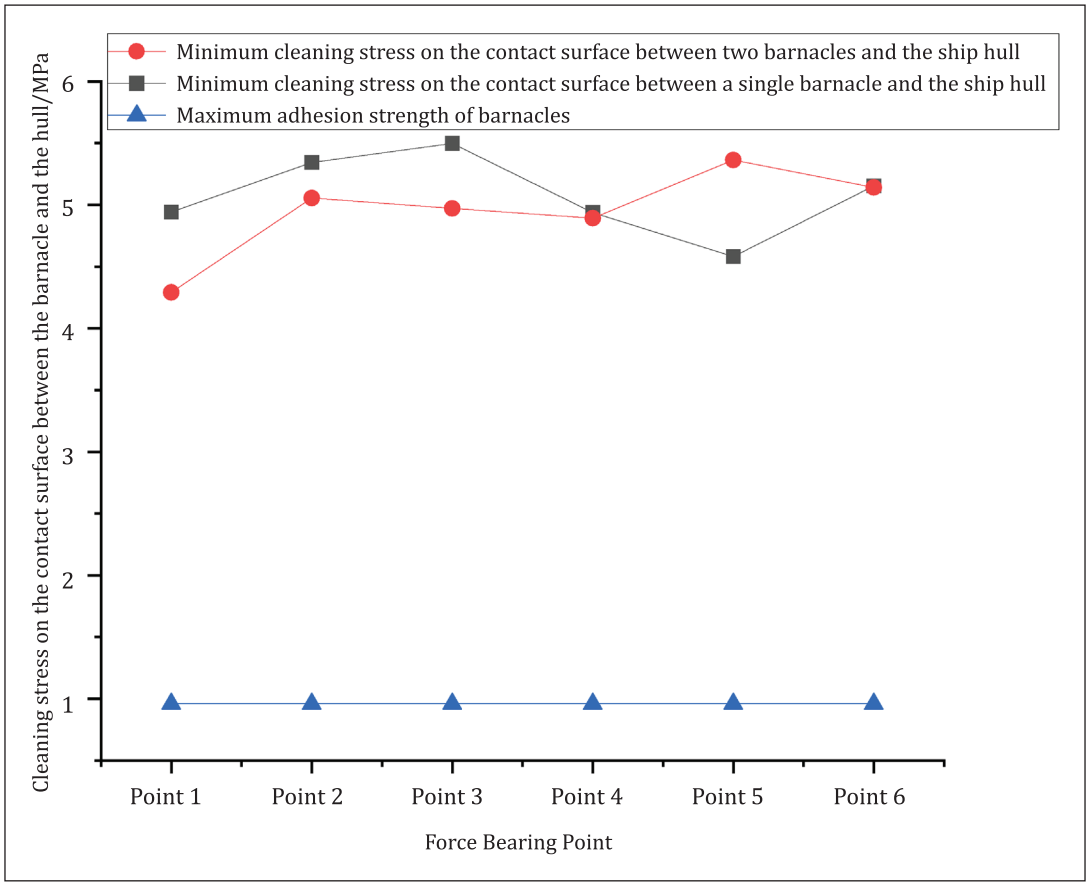

Figure 7 Minimum cleaning stress line generated by different stress points of double barnacles.

nacle and the hull, with only minor differences between the two conditions. This indicates that the cleaning blade provides sufficient stress to overcome the adhesive bonding and achieve effective detachment, regardless of whether a single barnacle or two adjacent barnacles are present. A detailed comparison shows that the minimum cleaning stress in the single-barnacle model occurs at Point 5, while that of the double-barnacle model appears at Point 1. This suggests that the presence of a neighboring barnacle has a localized influence on the stress distribution; however, the minimum stress remains well above the maximum adhesion strength, ensuring continuous and stable cleaning performance. Furthermore, Fig. 7 demonstrates that the cleaning blade maintains a uniform stress distribution in the double-barnacle scenario, guaranteeing cleaning efficiency and operational reliability under multi-barnacle attachment conditions. Therefore, the blade-based cleaning technology not only effectively removes individual barnacles but also sustains stable performance when dealing with clustered fouling, making it more suitable for efficient barnacle removal in engineering applications compared with ultrasonic cavitation.

The above results confirm that the cleaning blade exhibits stable stress characteristics and strong detachment capability when removing both single and paired barnacles. To further investigate its applicability and cleaning performance under large-area and continuous operating conditions, it is necessary to extend the analysis to more realistic scenarios involving various barnacle distribution patterns and attachment conditions.

5 Simulation Study of the Cleaning Blade under Different Barnacle Distribution Conditions

The two-barnacle cleaning simulation demonstrates that when the cleaning blade acts on two adjacent barnacles simultaneously, the resulting stress level is comparable to that of the single-barnacle case, indicating that the mutual mechanical interference between neighbouring barnacles is not significant. This suggests that the blade can maintain stable cutting performance under localized multi-point cleaning conditions. However, in practical scenarios, the attachment morphology of barnacles on ship hulls varies in density and spatial arrangement, and the cleaning blade will inevitably encounter diverse distribution patterns during operation. To further analyze the force characteristics and cleaning effectiveness of the blade under different attachment

configurations, three simulations were conducted based on the double-barnacle model: collinear distribution, staggered distribution, and dense multi-barnacle distribution. These simulations are intended to investigate the influence of barnacle arrangement on cleaning stress distribution and removal performance.

5.1 Cleaning of Collinear Barnacle Distribution

A collinear cleaning simulation model was established in ABAQUS, in which the cleaning blade performs a constant-speed linear translation along the hull surface, replicating the continuous sliding motion observed during actual cleaning operations. The blade rake angle was set to 20°, maintaining a constant contact angle with the hull surface to ensure a stable cutting force direction. Since Point 1 is closer to the interface between the barnacle cement layer and the hull, it more accurately reflects the stress state at the adhesion boundary during blade operation. This feature makes it suitable for analyzing effective stress transmission and barnacle detachment behavior. Therefore, to investigate the force evolution and removal mechanism during continuous cleaning, four barnacle models with equal spacing were arranged along the cleaning path, and Point 1 was selected as the blade–barnacle contact position, as illustrated in Fig. 8.

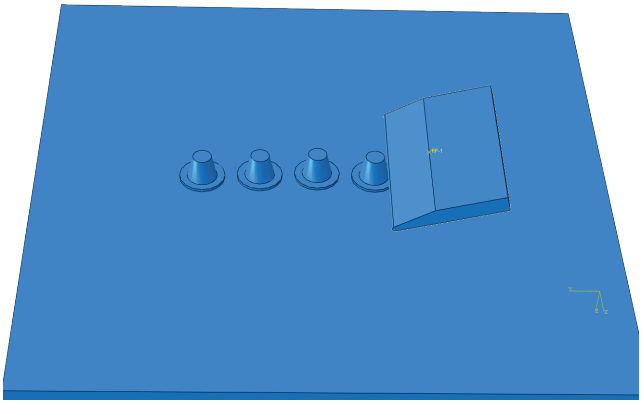

Figure 8 Finite element model of collinear barnacle distribution.

As shown in the four simulation results in Figure 9, when the rake angle of the cleaning blade is set to 20° and the blade performs continuous motion along the hull surface, it can stably penetrate the interface be-

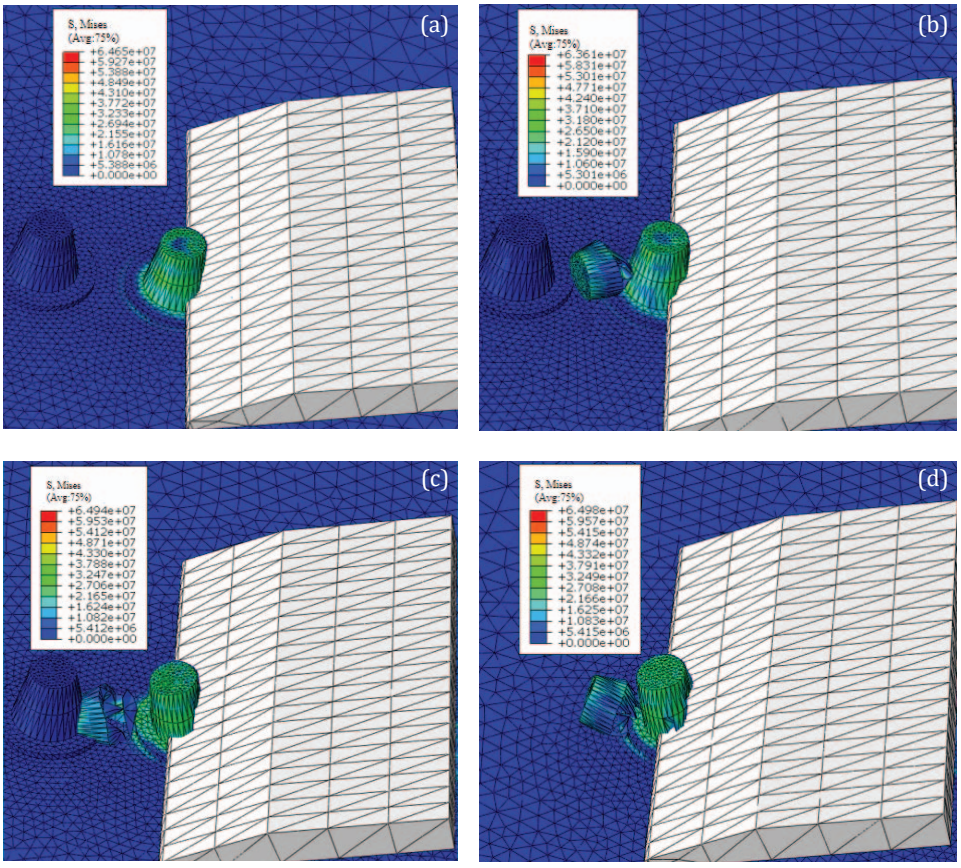

Figure 9 Cleaning stress distribution during collinear barnacle removal: (a) the cleaning blade contacts the first barnacle; (b) the cleaning blade contacts the second barnacle; (c) the cleaning blade contacts the third barnacle; (d) the cleaning blade contacts the fourth barnacle.

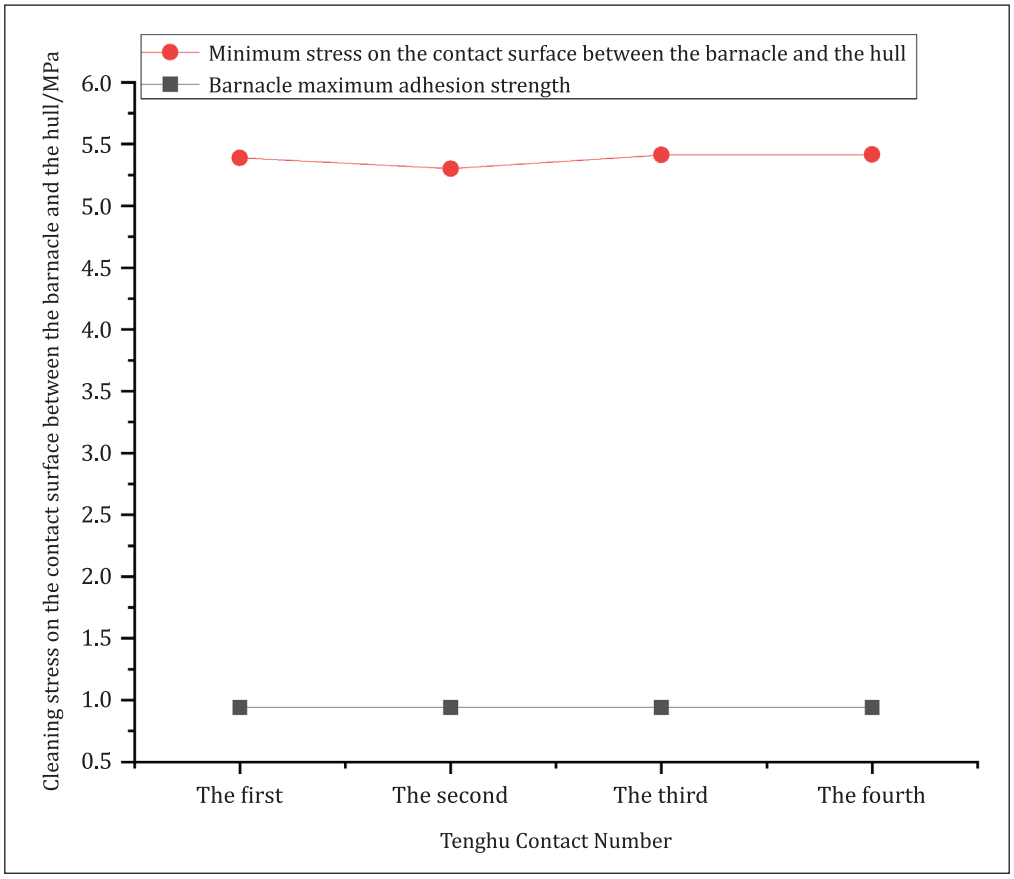

Figure 10 Stress variation curve for the collinear barnacle removal process.

tween the barnacle shell and the hull coating, thereby achieving effective overall barnacle detachment. During the cleaning process, the force acting on the blade remains smooth without noticeable rebound or sliding, indicating that the selected rake angle provides a favorable cutting condition that ensures both continuity and stability of the cleaning operation.

Further evidence can be obtained from the stress distribution curve in Figure 10, where the stress variations experienced by multiple barnacles along the collinear path exhibit a consistent trend with minimal fluctuation. This demonstrates that the blade can maintain a uniform force distribution under collinear attachment conditions. The minimum stress value reaches 5.3 MPa, which is approximately five times the maximum adhesion strength between the barnacle and the hull surface. This confirms that the stress applied by the blade is sufficient to overcome the barnacle adhesion force and achieve efficient removal. Meanwhile, the stress remains primarily concentrated within the barnacle shell and the adhesion interface, with minimal impact on the hull substrate, thereby ensuring both the safety and reliability of the cleaning process.

5.2 Staggered Arrangement Cleaning

In ABAQUS, a simulation model of barnacle removal with a staggered arrangement was established, in which the cleaning blade moves at a constant velocity along the hull surface to reproduce the sliding-cleaning process encountered in practical operations. The rake angle of the blade was again set to 20°, ensuring stable contact with the hull surface and maintaining a consistent force direction. Unlike the collinear arrangement, the barnacles in this model were positioned in a staggered pattern, where the centers of adjacent barnacles were laterally offset from the cleaning path. This configuration better reflects the non-uniform distribution of barnacles on actual ship surfaces and facilitates the analysis of force variations and stress transmission characteristics when multiple targets are engaged in a non-collinear manner. During the simulation, the cleaning blade started from a fixed initial position and sequentially engaged each staggered barnacle, enabling the study of the stress response and its influence on removal effectiveness under a non-collinear distribution, as shown in Fig. 11.

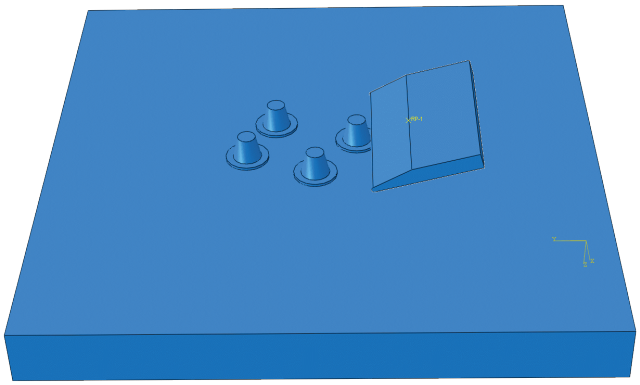

Figure 11 Staggered-arrangement cleaning simulation model.

From the simulation process shown in Fig. 12, it can be observed that when the rake angle of the blade is set to 20°, the cleaning blade model is able to effectively remove barnacles arranged in a random staggered pattern. As the blade sequentially engages barnacles located at different positions along the cleaning path, the adhesion interface between the barnacle shell and the hull surface is progressively destroyed, indicating that the cleaning stress generated by the blade is sufficient to overcome the maximum adhesion strength of the barnacles and achieve stable detachment. This demonstrates that variations in the spatial distribution of barnacles do not cause a significant negative effect on the cleaning outcome, and the removal process remains stable throughout.

A further comparison of the stress evolution trends between collinear and staggered cleaning, as illustrated in Fig. 13, shows that in both conditions the cleaning stress remains at approximately 5 MPa, which is about five times higher than the adhesion strength of the barnacles. This level of stress is sufficient to ensure reliable detachment in both cases. Although the stress in the collinear arrangement is slightly higher than that in the staggered arrangement, the difference is minor, and both conditions satisfy the critical requirement for barnacle removal. These results indicate that the proposed cleaning blade technology maintains stable cleaning performance under different barnacle distribution patterns and can effectively accommodate force variations

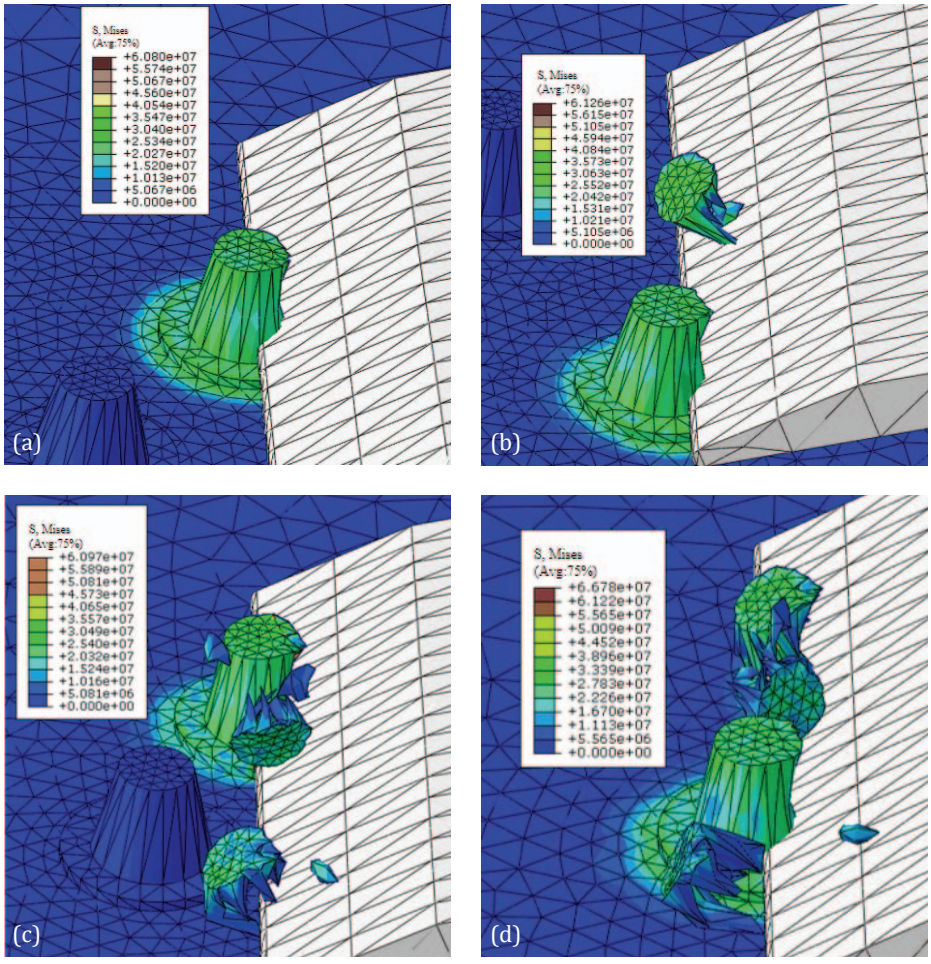

Figure 12 Cleaning stresses generated during collinear barnacle removal: (a) blade contacting the first barnacle; (b) blade contacting the second barnacle; (c) blade contacting the third barnacle; (d) blade contacting the fourth barnacle.

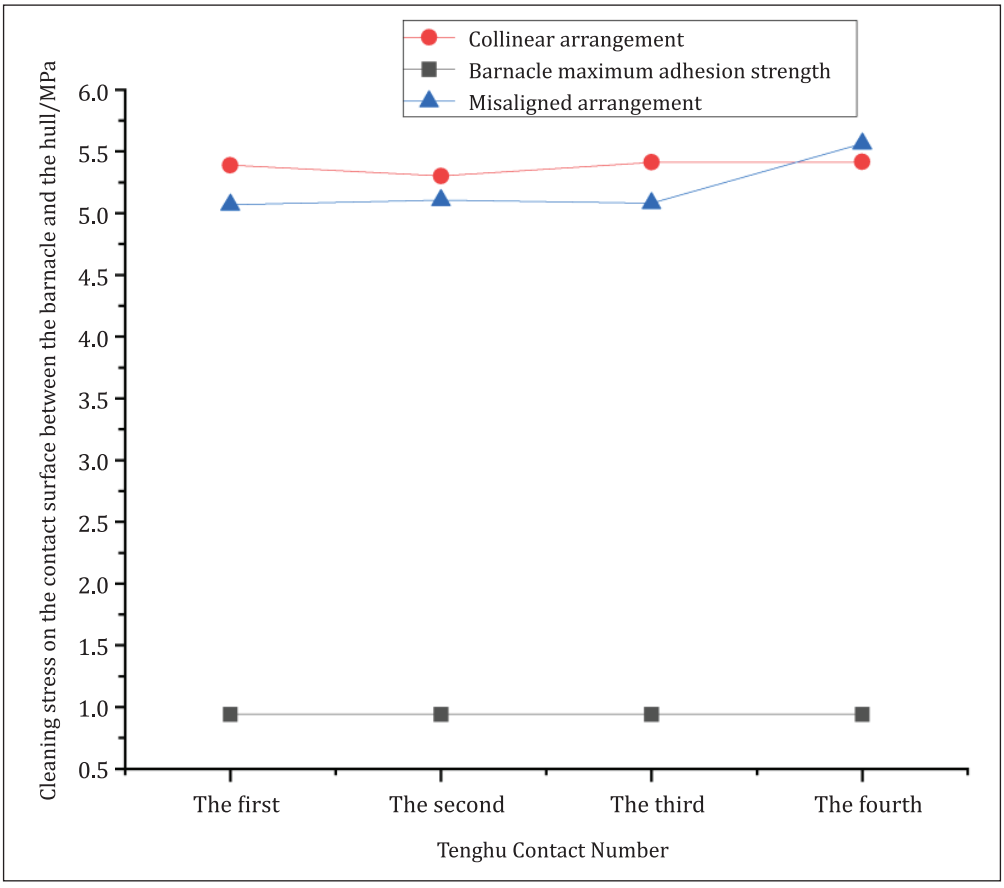

Figure 13 Comparison of stress variation between collinear and staggered barnacle-removal conditions.

caused by multi-body staggered arrangements, ensuring continuity and reliability in the cleaning process. The staggered-arrangement simulation verifies the adaptability of the cleaning blade under non-collinear and multi-target conditions, providing theoretical and simulation support for subsequent investigations of large-area cleaning scenarios involving dense barnacle fouling.

5.3 Dense Distribution Cleaning

On actual ship hull surfaces, barnacles are typically distributed in large-scale dense patterns, which significantly increase interaction effects and stress superposition during the cleaning process. To further evaluate the stability and adaptability of the proposed cleaning blade under complex fouling conditions, a dense multi-barnacle distribution model is constructed based on the collinear and staggered arrangements. In this scenario, a 200 mm × 200 mm hull surface area is considered, within which twelve barnacles are randomly distributed, corresponding to an attachment density of approximately 300 barnacles/m^2. This density falls within a reasonable and relatively conservative range for high-density fouling conditions commonly observed below the ship waterline, allowing the interaction and stress superposition effects to be effectively captured while avoiding numerical instability associated with excessively high attachment densities. All other simulation conditions remain consistent with those of the previous two arrangement cases, and the corresponding model is shown in Fig. 14.

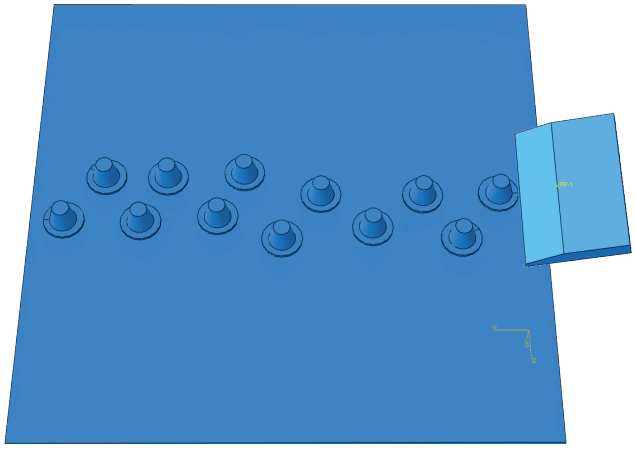

Figure 14 Dense-distribution cleaning simulation model.

Fig. 15 shows the stress distribution during the cleaning of densely distributed barnacles. Specifically, Fig. 15(a) illustrates the stress field when the tool engages the first barnacle, while Fig. 15(b) and Fig. 15(c) present

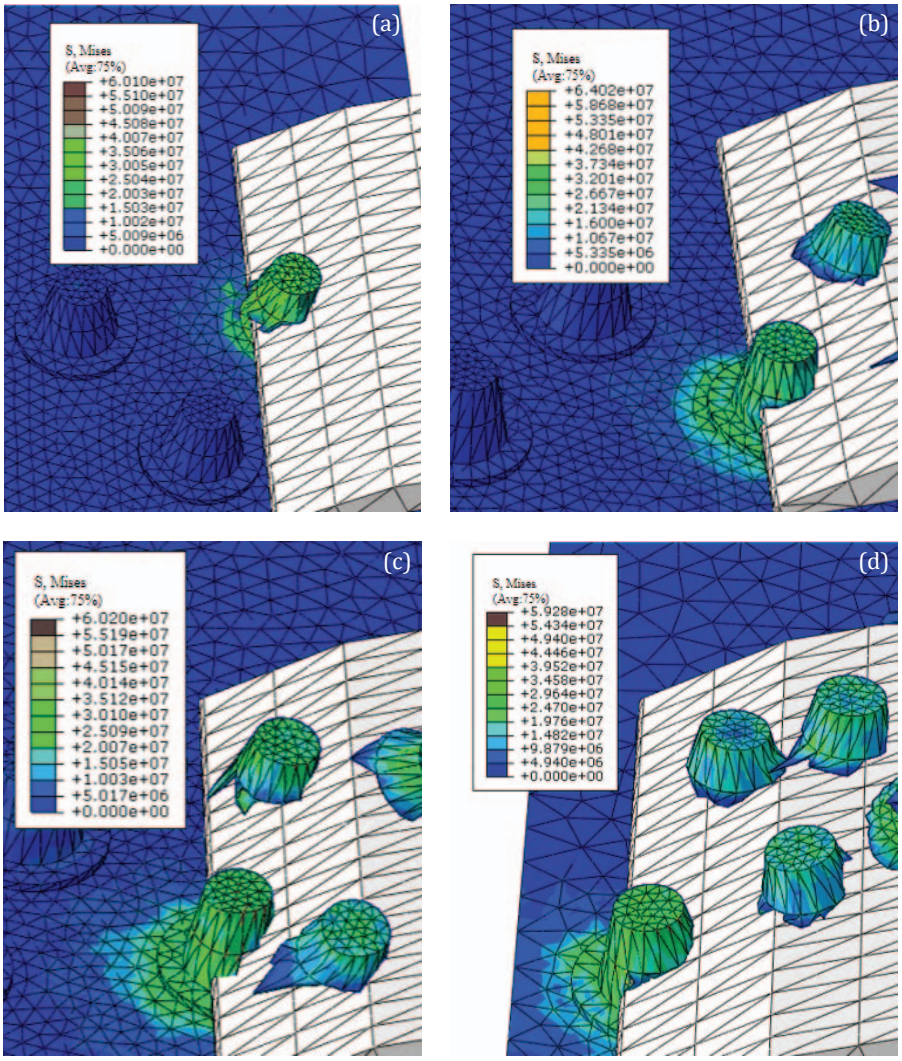

Figure 15 Clean stress generated during dense-distribution barnacle cleaning: (a) contact between the cleaning blade and the first barnacle; (b) contact with the barnacle at one-third of the path; (c) contact with the barnacle at two-thirds of the path; (d) contact with the last barnacle.

the stress distribution when the cleaning blade interacts with barnacles located in the central region of the dense cluster. Fig. 15(d) displays the stress response when the tool removes the final barnacle in the distribution. As shown in Fig. 15(a-d), when the rake angle of the tool is set to 20°, the stress at the tool-barnacle interface remains within the range of 4.9-5.4 MPa, which is significantly higher than the maximum adhesion strength of barnacles. This indicates that the proposed cleaning-blade model maintains sufficient debonding capability even under densely distributed attachment conditions. Moreover, the simulation results in Fig. 15 demonstrate that as the blade slides along the hull surface, multiple adjacent barnacles are sequentially removed within a short period. This confirms that the cleaning blade exhibits good cutting stability and operational continuity when cleaning barnacles in high-density fouling scenarios.

As shown in Fig. 16, under the three different barnacle distribution conditions, the average cleaning stress acting on the barnacles remains approximately 5 MPa, which is more than five times the maximum adhesion strength of the barnacles. This indicates that the proposed cleaning-blade model can provide sufficient debonding capability under collinear, staggered, and densely distributed barnacle arrangements, effectively overcoming the adhesion between barnacles and the hull and achieving thorough removal of adult barnacles. Moreover, the variation in average stress across the three distribution modes is minimal, demonstrating that the cleaning blade can maintain stable cutting forces and continuous cleaning performance under different fouling arrangements, providing a reliable basis for efficient removal of barnacles on realistically heterogeneous hull surfaces.

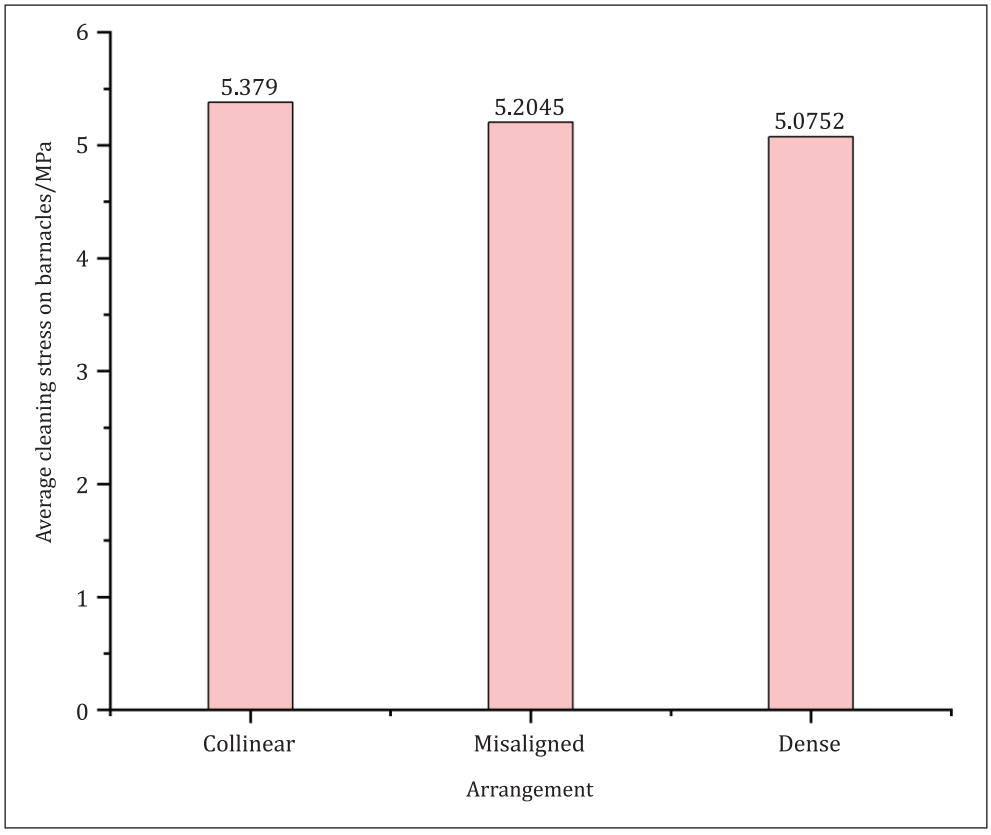

Figure 16 Average cleaning stress acting on barnacles under different distribution patterns.

6 Conclusions

To address the issue of barnacle removal from ship hulls, a dynamics model of the cleaning blade was established by combining classical cutting theory with the extrusion cutting method. The analysis results indicate that when the tool rake angle is 20°, the corresponding cutting force is close to the barnacle removal force, providing a reliable theoretical basis for subsequent finite element simulations.

An idealized adhesion model of barnacles on the hull surface was constructed, and finite element simulations were performed with the blade rake angle set to 20°. The results show that, under both single- and double-barnacle conditions, the cleaning stress produced by the blade is about four times greater than the barnacle adhesion strength. This confirms that the optimized blade can efficiently remove barnacles with stable performance while minimizing the additional drag and fuel consumption caused by fouling. Compared with ultrasonic cavitation technology used in conventional hull-cleaning robots, the proposed blade model demonstrates advantages in stress uniformity, energy efficiency, and cleaning consistency.

Further simulations under various barnacle distribution patterns—collinear, staggered, and densely clustered—show that the cleaning blade provides sufficient removal stress, with average values exceeding five times the barnacle adhesion strength. These results highlight the blade's capability to maintain high cleaning efficiency and uniform stress distribution across complex adhesion conditions, offering an environmentally sustainable and energy-saving approach for improving ship hydrodynamic performance and navigation efficiency.

Further simulations under various barnacle distribution patterns—collinear, staggered, and densely clustered—show that the cleaning blade provides sufficient removal stress, with average values exceeding five times the barnacle adhesion strength. These results highlight the blade's capability to maintain high cleaning efficiency and uniform stress distribution across complex adhesion conditions, offering an environmentally sustainable and energy-saving approach for improving ship hydrodynamic performance and navigation efficiency.

Funding: This research is funded by the following projects: Hainan University's high-level talent scientific research start-up fund [project number KYQD (ZR)-22060], and the National Natural Science Foundation – key project [project number 52231012].

Acknowledgments: The authors would like to express their sincere gratitude to the research group members for their valuable discussions and technical assistance

throughout the study. Special thanks are also extended to the State Key Laboratory of South China Sea Marine Resource Utilization for providing essential simulation facilities and technical support. The constructive feedback from colleagues greatly contributed to improving the quality of this work.

Author Contributions: Xiaochang Shi contributed to the conceptualization and methodology of this research, conducted model construction and numerical simulations, prepared the figures, and drafted the initial manuscript (Writing – Original Draft). Changsheng Yang was responsible for data collection and statistical analysis (Data Curation, Formal Analysis). Wenbin Ma secured project funding (Funding Acquisition), provided academic supervision (Supervision), and contributed to the revision, finalization, and language editing of the manuscript (Writing – Review & Editing). All authors have read and approved the final version of the manuscript and agree to be accountable for all aspects of the work.

References

[1] Chen, C., L. Xiang, and H. Liu, *Attachment and prevention of marine fouling barnacles.* Marine Environmental Science, 2012. **31**(4): p. 621–624.

[2] Song, C. and W. Cui, *Review of underwater ship hull cleaning technologies.* Journal of marine science and application, 2020. **19**(3): p. 415–429.

[3] Scianni, C. and E. Georgiades, *Vessel in-water cleaning or treatment: identification of environmental risks and science needs for evidence-based decision making.* Frontiers in Marine Science, 2019. **6**: p. 467.

[4] Bloecher, N., T. Solvang, and O. Floerl, *Efficacy testing of novel antifouling systems for marine sensors.* Ocean Engineering, 2021. **240**: p. 109983.

[5] Wang, J., Z. Zhang, and H. Liu, *Current Status and Key Technological Advances of Underwater Cleaning Robots for Marine Organisms on Ship Hulls.* Ship Engineering, 2024. **46**(2): p. 146–164.

[6] Eich, M., et al., *A robot application for marine vessel inspection.* Journal of Field Robotics, 2014. **31**(2): p. 319–341.

[7] Hachicha, S., et al., *Innovative design of an underwater cleaning robot with a two arm manipulator for hull cleaning.* Ocean Engineering, 2019. **181**: p. 303–313.

[8] Luo, G., et al., Shape Optimization of Cleaning Robot for Ships Based on Bezier Curve and Improved Optimization Algorithm. International Journal of Computational Fluid Dynamics, 2025: p. 1–19.

[9] Haugaløkken, B.O., et al. Docking stations for net-crawling underwater vehicles in aquaculture net pens. in OCEANS 2021: San Diego–Porto. 2021. IEEE.

[10] Liu Jianguo, et al., Overview of the Development of Water Jet Propulsion Technology Ship, 2023 34(06): p. 1.

[11] Sun Chuan et al., Hydrodynamic Characteristics Analysis of a Negative Pressure Adsorption Device Based on CFD Journal of Mechanical & Electrical Engineering, 2020. 37(2).

[12] Harbin BanZhiLan Marine Technology Co., L. *BanZhiLan Marine "BLUCR" Robots No. 3 and No. 4 Successfully Launched.* 2024–06–19; Available from: https://www.banzhilan.com/newsinfo/4740630.html.

[13] Tianjin Hanhai Lanfan Marine Technology Co., L. *Actual Measurement Efficiency of Multibeam Echo Sounding System on Ship and Dam Cleaning Robots.* 2024–06–19; Available from: http://tjhhlf.com/sys-nd/12.html.

[14] Wang, L., et al., *Mechanical Study on the Removal of Adhered Barnacles by Marine Steel Pile Cleaning Robots.* Journal of Harbin Engineering University, 2021. **42**(2): p. 259–265.

[15] Xia, H., *Study on the Patterns of Marine Biofouling on Ship Surfaces and Cleaning Robots*. 2018, Harbin Engineering University.

[16] Li, J., *Structural Design and Performance Analysis of a Composite Suction-type Underwater Hull Cleaning Robot* 2023, Yantai University.

[17] SHA, Z., et al., *Research on cutting force of extrusion cutting process based on material flow characteristics.* Journal of Manufacturing Processes, 2024. **122**: p. 83–96.

[18] Albitar, H., et al., *Underwater robotics: surface cleaning technics, adhesion and locomotion systems.* International Journal of Advanced Robotic Systems, 2016. **13**(1): p. 7.